Extended SO2outgassing from the 2014â2015 Holuhraun lava flow field, Iceland

Extended SO_2 outgassing from the 2014-2015 Holuhraun lava flow field, Iceland

Isla C. Simmons[1], Melissa A. Pfeffer[2], Eliza S. Calder[1], Bo Galle[3], Santiago Arellano[3], Diego Coppola[4], Sara Barsotti[2]

1. School of GeoSciences, The University of Edinburgh, Edinburgh, United Kingdom
2. Icelandic Meteorological Office, Reykjavík, Iceland
3. Department of Space, Earth and Environment, Chalmers University of Technology, Gothenburg, Sweden
4. Department of Earth Science, University of Torino, Torino, Italy

Contact details

Isla Simmons, isla.simmons@ed.ac.uk

ORCID

Isla Simmons: 0000-0002-3959-5772

Melissa Pfeffer: 0000-0002-1689-1739

Eliza Calder: 0000-0002-1644-2087

Santiago Arellano: 0000-0002-0306-3782

Abstract

The 2014-2015 Holuhraun eruption was the largest fissure eruption in Iceland in the last 200 years. This flood basalt eruption produced ~1.6 km^3 of lava, forming a lava flow field covering an area of ~84 km^2. Over the six-month course of the eruption ~11 Mt of SO_2 were released from the eruptive vents as well as from the cooling lava flow field. This work examines the post-eruption SO_2 flux emitted by the Holuhraun lava flow field, providing the first study of the extent and relative importance of the outgassing of a lava flow field after emplacement.

We use data from a scanning differential optical absorption spectroscopy (DOAS) instrument installed at the eruption site to monitor the flux of SO_2. In this study, we propose a new method to estimate the SO_2 emissions from the lava flow field, based on the characteristic shape of the scanned column density distribution of a homogenous source close to the ground. Post-eruption outgassing of the lava flow field continued for at least three months after the end of the eruption, with SO_2 flux between <1 kg/s and 9 kg/s. The lava flow field post-eruption emissions were not a significant contributor to the total SO_2 released during the eruption, however the lava flow field was still an important polluter and caused high concentrations of SO_2 at ground level after lava effusion ceased.

Keywords SO_2, lava, DOAS, post-eruption outgassing

Introduction

A dyke-fed basaltic fissure eruption from the Bárðarbunga volcanic system occurred from 31 August 2014 until 27 February 2015 (Icelandic Meteorological Office (IMO), 2015a). The fissure was located to the north of the Vatnajökull icecap, forming the 2014-2015 Holuhraun lava flow field (Figure 1). The eruption produced 1.6 ± 0.3 km^3 of lava, forming an 84.1 ± 0.6 km^2 lava flow field (Gíslason et al., 2015). This classifies the eruption as a flood basalt eruption following Thordarson and Larsen (2007). This makes the Holuhraun eruption the most voluminous effusive eruption in Iceland since the 1783-1784 Laki eruption (Schmidt et al., 2015).

This work provides a new approach for measuring SO_2 emissions from a lava flow field after emplacement. Several studies have investigated the impacts of the Holuhraun eruption on populations and the environment (e.g. Gislason et al., 2015; Ilyinskaya et al., 2017). Establishing the potential duration and magnitude of post-eruptive SO_2 outgassing will increase resilience in vulnerable communities related to the health hazards caused by SO_2 after future eruptions. We additionally discuss the physical processes of cooling and fracturing (e.g. Keszthelyi and Denlinger, 1996; Kattenhorn and Schaefer, 2008; Patrick et al., 2004; Wittmann et al., 2017) that contribute to post-emplacement lava outgassing.

Volatile outgassing during and after eruption

Gases dissolved within magma are transferred to the atmosphere by degassing. The term "degassing" is used to describe the process by which a magma loses its volatiles (Burgisser and Degruyter, 2015). This includes exsolution of gas from the melt, gas segregation, and outgassing (e.g. Bottinga and Javoy, 1991; Sparks, 2003; Palma et al., 2008). Following

63 Burgisser and Degruyter (2015) and Palma et al. (2008; 2011) we define "outgassing" only as
64 the release of this gas to the atmosphere.

65 Basaltic fissure eruptions release large volumes of SO_2 into the atmosphere. Basaltic magmas
66 have a high sulphur yield, which is typically two to four times higher than silicic magmas
67 (Thordarson et al., 2003). As a result, SO_2 is released during basaltic flood eruptions by a two-
68 stage degassing process: from the magma as it rises through the conduit and erupts at the vent,
69 and from lava flows during and after their emplacement (Walker, 1989; Thordarson et al., 1996;
70 Thordarson et al., 2003). Gases released at the vent, and associated with degassing of volatiles
71 as the magma approaches the surface, contribute to an eruption plume. Gases released from
72 lava flows will remain close to ground level forming a low-level haze (Figure 2).

73 Swanson and Fabbi (1973) studied volatile loss during isothermal flowage of pahoehoe lava in
74 lava tubes at Mauna Ulu, Hawaii. They observed that the majority of sulphur was released soon
75 after eruption (60% was lost during flowage over a distance of 12 km), but lava flows were
76 observed to continue outgassing for at least two to four hours after solidification (Swanson and
77 Fabbi, 1973). In contrast, the Holuhraun lava flow field exhibits a wide range of lava
78 morphologies, varying from pāhoehoe to 'a'ā (Pedersen et al., 2017) and, as demonstrated by
79 this work, continued to release sulphur volatiles for several months after emplacement.

80 In another study on Hawaiian flows, Bottinga and Javoy (1991) proposed that lava flows degas
81 volatiles during transportation because their temperature decreases. The resulting
82 supersaturation of volatiles within the lava increases, causing exsolution resulting in bubble
83 formation. Cashman et al. (1994) proposed that volatiles were primarily released from active
84 lava flows by the rise and escape of bubbles already contained within the lava. Sparks and
85 Pinkerton (1978) noted that as lava is degassed, exsolution of gas results in undercooling of the
86 lava. This leads to crystallisation, and causes an increase in viscosity and yield strength (Sparks

87 and Pinkerton, 1978). Mechanical processes during the flowage of lava then cause the solidified
88 crust to fracture (e.g. Polacci and Papale, 1997; Soule and Cashman, 2004), allowing further
89 gas to be released.

90 Many studies have investigated the degassing of lava flows as they are actively flowing from
91 the vent, however little discussion exists about the processes of extended outgassing following
92 lava flow emplacement. The studies of Bottinga and Javoy (1991) and Cashman et al. (1994)
93 both examine the release of gases from flowing lava and are therefore insufficient to explain
94 the continued flux of SO_2 from the Holuhraun lava flow field for several months after its
95 emplacement and solidification. We thus, here, consider the physical processes which occur
96 over the longer time period that was captured by our outgassing measurements.

97

98 *Volcanic SO_2 monitoring*

99 SO_2 emission measurements have been fundamental to volcano monitoring since the
100 development of the correlation spectrometer (COSPEC) in the 1970s (Moffat and Millan, 1971;
101 Stoiber et al., 1983). Malinconico (1979) observed that increases in SO_2 flux at Mt Etna, Italy,
102 corresponded to increases in volcanic activity, suggesting that SO_2 fluctuations can be used to
103 predict eruptions. SO_2 flux has since been observed to correlate with volcanic activity
104 (Soufrière Hills, Montserrat; Edmonds et al., 2003), magma extrusion rate (Unzen, Japan;
105 Hirabayashi et al., 1995), seismicity during explosive activity (Merapi, Indonesia; Jousset et
106 al., 2013) and lava lake activity (Villarrica, Chile; Palma et al., 2008, and Erebus, Antarctica;
107 Kyle et al., 1994).

108 Differential optical absorption spectroscopy (DOAS) was also developed in the 1970s, as a
109 method for measuring atmospheric gases (Platt et al., 1979). It has since been used to measure

110 SO_2 emissions of volcanoes worldwide (e.g. Edner et al., 1994; Weibring et al., 1998;
111 McGonigle et al., 2002), and has now superseded COSPEC as the primary volcanic SO_2 flux
112 monitoring technique (Galle et al., 2002; Bobrowski et al., 2010). Measurement of volcanic
113 plumes was further enhanced by the development of the SO_2 camera (Mori and Burton, 2006;
114 Bluth et al., 2007), providing high temporal resolution SO_2 flux measurements and allowing
115 SO_2 heterogeneity within the plume to be quantified (Bluth et al., 2007). SO_2 measurement
116 techniques have been employed to determine SO_2 emissions within volcanic plumes, both
117 during eruptive episodes (e.g. Jousset et al., 2013; Gíslason et al., 2015) and during passive
118 degassing (e.g. McGonigle et al., 2002; Sawyer et al., 2008), however this work provides the
119 first attempt at using DOAS to measure the SO_2 released by an emplaced lava flow field.

120

121 *The 2014-2015 Holuhraun eruption*

122 Over the six month course of the Holuhraun eruption, 11 ± 5 Mt of SO_2 were emitted (Gíslason
123 et al., 2015), with average emission rates of 400 kg/s, and peaks of over 1000 kg/s (Barsotti et
124 al., 2015; Gauthier et al., 2016). The majority of gases were released from the eruption fissure
125 and contributed to an eruption plume that contained very little ash but was concentrated in SO_2
126 and H_2O (Gíslason et al., 2015). In addition to the principal eruption plume, SO_2 was also
127 released directly from the lava flows, forming a low-level haze of SO_2. A surveillance flight
128 on 4 November 2014, for example, revealed a distinct two-layered gas cloud that included a
129 low-level "haze" of H_2O (both magmatic and meteoric), SO_2 and other volcanic gases. This
130 haze rose from the lava flow field to an elevation of 700 m above ground level, with the
131 eruption plume ascending to an elevation of 1500-2500 m (Figure 3; IMO, 2014). High
132 concentrations of SO_2 were measured at ground level throughout Iceland, and in many
133 communities the health standard of 350 $\mu g/m^3$/hr was exceeded, posing health risks to the

134 population (Gíslason et al., 2015, Ilyinskaya et al., 2017). After the eruption ceased at the end
135 of February 2015, high concentrations of SO_2 continued to be detected at ground level near to
136 the eruption site, but dropped to background levels at communities downwind (IMO, 2015a;
137 Umhverfisstofnun, 2016). The aim of this work was to measure the SO_2 released from the
138 cooling lava flow field after the eruption, and to examine the processes that facilitate an
139 emplaced, cooling lava flow field to outgas over a prolonged period.

140

141 **Methods**

142 The methodology used to derive the SO_2 flux from the lava flow field was based on the same
143 principle as is used in COSPEC and MobileDOAS measurements of an elevated gas plume (e.g.
144 Stoiber et al., 1983; Galle et al., 2002). Following this approach, the vertical column density
145 (VCD) of a gas is measured using absorption spectroscopy with the sky as the light source
146 (Platt and Stutz, 2008). By traversing under the plume in a direction approximately
147 perpendicular to the plume propagation, and integrating the obtained vertical column amounts,
148 the total number of molecules in a cross-section of the plume may be determined. After
149 multiplication with the plume speed the total gas emission is calculated (e.g. Edner et al., 1994;
150 Galle et al., 2002; McGonigle et al., 2002; Edmonds et al., 2003; Platt et al., 2015).

151 In our application, a stationary scanning DOAS instrument (ScanDOAS; Galle et al., 2010)
152 was used to determine the VCD of the low-level haze of gas emitted by the lava flow field. To
153 make this measurement we assume that the lava flow field produces a gas layer close to the
154 ground with uniform thickness. We also assume that this layer has a width that is equal to the
155 maximum width of the lava flow field, measured in a direction perpendicular to the wind
156 direction, the “effective haze width”. Using this geometry, with a ScanDOAS instrument we
157 can determine the VCD at the instrument location, and using the known wind direction and

158 shape of the lava flow field we can derive the effective haze width. The gas flux can then be
159 determined by multiplying the VCD at the instrument site with the effective haze width and
160 with the wind speed.

161

162 *Measurement geometries*

163 A ScanDOAS scans the sky from horizon to horizon in a vertical plane approximately
164 perpendicular to the plume propagation, recording radiance spectra of the diffused UV solar
165 radiation received at each angle (Edmonds et al., 2003). The "slant column density" (SCD) of
166 SO_2 from each spectrum is calculated by differential optical absorption spectroscopy (DOAS),
167 and the integral of column densities at all angles is then multiplied by the plume speed to obtain
168 the flux of SO_2 (e.g. Stoiber et al., 1983; Galle et al., 2002; McGonigle et al., 2002). The
169 instrument typically makes one scan approximately every five minutes, each scan being
170 composed of 26 spectra.

171 In a variation on this "flat" scan geometry, the scan is made over a conical surface with its tip
172 at the instrument and its base through the gas source. The main advantage of this "conical"
173 geometry is that a wider range of plume directions may be covered by a single instrument
174 (Galle et al., 2010). In this study, a conical geometry with an opening angle of 60^o was used.
175 The instrument used in our study is a modification of the standard NOVAC-Mark I instrument
176 (NOVAC: Network for Observation of Volcanic and Atmospheric Change; Galle et al., 2010),
177 with a non-rotating, cylindrical external hood made of quartz, and a UV sensitive OceanOptics
178 MAYA Pro spectrometer (http://oceanoptics.com/wp-content/uploads/OEM-Data-Sheet-
179 Maya2000Prov3.pdf).

180 SO_2 emissions from a vent will contribute to an elevated eruption plume, which will be
181 identified on a DOAS scan as a concentrated distribution of SO_2 column densities, with higher
182 columns observed at elevation angles in which the scanner detects the bulk of the plume (Figure
183 4a). In contrast, SO_2 emissions from a lava flow field or a grounded plume will form a dispersed
184 low-level haze. This will have a characteristic trough shape on a DOAS scan (Figure 4b). When
185 scanning through a low-level haze of SO_2, the optical path will be greater at low elevation
186 angles close to the ground, producing a greater SO_2 slant column density. The minimum slant
187 column densities of SO_2 will be observed at the highest elevation angles, where the shortest
188 path through the haze is sampled (Figure 4b). With flat geometry this occurs at zenith, but for
189 the conical geometry used here this condition is met at 30^o from zenith.

190

191 *Determination of the SO_2 vertical column density at the measurement site*

192 If we assume a layer of gas close to the ground, and flat scan geometry, then the slant column
193 densities (SCD) can be expressed as:

194 $$SCD = VCD/\cos(\alpha) \quad (1)$$

195 where VCD is the vertical column density through the sampled layer and α is the scan angle
196 measured from the zenith.

197 In a standard evaluation of a DOAS spectrum, the spectrum measured through the gas plume
198 is divided by a clean air reference spectrum, typically obtained in a direction with no gas (Galle
199 et al., 2002; Edmonds et al., 2003). In this way spectral features related to the sky spectra as
200 well as instrumental features are cancelled out and an absorption spectrum of the gas plume is
201 obtained. When scanning through a low-level haze, all spectra, including the reference
202 spectrum, will contain SO_2. Our goal was therefore to determine the VCD without having

203 access to a clean air reference spectrum. In this case, the derived slant column was the
204 difference between the slant column of the measured spectrum and the slant column of the
205 reference spectrum by which it was divided. For a flat geometry this can be achieved by
206 dividing a spectrum taken at $\alpha = 60^o$ with a reference spectrum taken at $\alpha = 0^o$. The resulting
207 $SCD_{diff} = VCD/0.5 - VCD/1 = VCD$, provides the required VCD.

208 For a conical geometry the same method can be applied. However here the relation between
209 VCD and SCD becomes:

210 $$SCD = VCD/[\cos(\alpha) \times \sin(\beta)] \quad (2)$$

211 With the conical angle $\beta = 60°$, the difference between the SCD taken at angles $\alpha = 60°$ and α
212 $= 0°$ becomes:

213 $$SCD_{diff} = VCD/0.866 \quad (3)$$

214 Therefore, to obtain the VCD at the instrument location we multiply the average SCD obtained
215 at angles $\alpha = 60°$ and $\alpha = 0°$ by 0.866. The SCD and VCD are, by convention, expressed in
216 ppm*m (parts per million-metre). To calculate SO_2 emission, these are converted to kg/m^2 by
217 applying the ideal gas law and multiplying the VCD (in ppm*m) by 2.66×10^{-6}.

218

219 *Field configuration and SO_2 flux calculation*

220 ScanDOAS instruments were installed at the Holuhraun eruption site by the Icelandic
221 Meteorological Office and Chalmers University to measure SO_2 emissions during the eruption.
222 Instrument MAYP111126 (cross symbol in Figure 1) was installed at its location to the east of
223 the lava flow field on 4 March 2015, where it was oriented towards the west and optimally
224 located for viewing of the lava flow field. This occurred after the eruption ended on 27 February,

and data from this spectrometer were used to calculate the post-eruptive SO_2 flux from the lava flow field.

All scans from instrument MAYP111126, from its installation on 4 March 2015 until 31 May 2015, were examined to identify those with the characteristic trough shape that represented the anticipated view through a low-level haze of SO_2 from the lava flow field (Figure 4c). Each "haze" scan was first re-evaluated between 310 nm and 325 nm using the NovacProgram software (version 1.82; Galle et al., 2010), including additional spectra in the DOAS fitting process to account for the presence of ozone in the atmosphere and the "Ring effect" (i.e. the "filling-in" of deep absorption features, such as the solar Fraunhofer lines, in a measured atmospheric spectrum, which is caused by inelastic (Raman) scattering of light by air molecules (Grainger and Ring, 1962)). After calculating the column densities, a quality check was applied to ensure that scans retained the characteristic trough shape of the anticipated lava flow field "haze" scans. To ensure a symmetrical trough shape, scans were excluded if slant column densities at +60° and -60° differed by more than 20%. To calculate the SO_2 flux (in kg/s) recorded by each scan, the measured VCD of SO_2 (in kg/m^2) was multiplied by the effective width of the SO_2 haze (in m) and the haze speed (in m/s), assumed to be equivalent to the wind speed measured at a co-located meteorological station.

As mentioned above, the effective width of the low-level haze produced by the lava flow field was assumed to be equal to the total width of the lava flow field, measured in a direction perpendicular to the wind direction (Figure 5). Because the lava flow field has an irregular shape, this width varies with different wind directions, and can be measured from a map showing the extension of the lava flow field. The minimum effective haze width occurs when the wind blows along the longer dimension of the lava flow field, and as wind direction deviates from this the effective haze width increases (Figure 5).

Wind speed and direction were recorded every 10 minutes using a meteorological station installed at the eruption site. Scans were filtered by wind direction, with scans included only when the wind was blowing towards the instrument (± 20°).

Lava flow field radiant heat flux

The radiant heat flux of the Holuhraun lava flow field was estimated using MODIS (Moderate Resolution Imaging Spectroradiometer), elaborated by the MIROVA (Middle InfraRed Observation of Volcanic Activity) system of Coppola et al. (2016). During the effusive crisis, the MIROVA system allowed automatic measurements of the volcanic radiative power (VRP) sourced from the active lava flow field, and related effusion rates (Coppola et al., 2017). However, the VRP provided automatically by MIROVA is based on the simple heat flux conversion approach of Wooster et al. (2003), that works for active lava flows with high surface temperatures (>600 K). This approach begins to fail for cooling surfaces, especially below 200°C, which is the case of the post-eruption Holuhraun lava flow field. For this post-eruptive period we thus recalculate the radiant heat flux as:

$$Q_{rad} = \sigma \varepsilon A_{flow} (BT_{MIR,flow}^4 - BT_{MIR,bk}^4) \quad (4)$$

where σ is the Stefan-Boltzmann constant (5.67051×10^{-8} W m^{-2} K^{-4}), ε is the emissivity of the lava surface (assumed to be 0.95 for basalt; Patrick et al., 2004), A_{flow} is the final area of the cooling lava flow field (84 km^2; Pedersen et al., 2017), and $BT_{MIR,flow}$ and $BT_{MIR,bk}$ are the average brightness temperatures of the flow surface pixels and surrounding background respectively, calculated from selected MODIS-MIROVA cloud-free images (Figure 6).

271 *Uncertainty and error*

272 Individual SO_2 flux measurements were calculated as the product of the average vertical
273 column density (VCD), effective haze width and wind speed. Thus, the total uncertainty on the
274 flux measurement can be obtained by determining the uncertainties of these three
275 independently derived quantities. The uncertainty on the average VCD depends on two factors:
276 the intrinsic uncertainty of the retrieved SCDs at various angles and the uncertainty related to
277 the method used to derive the mean VCD from a set of SCDs in one scan. The typical
278 uncertainty of a DOAS SCD has been characterized for NOVAC instruments by Galle et al.
279 (2010) and is expected to be around 15%. The sources of this uncertainty include added UV
280 radiation by scattering between the plume and the instrument (Mori et al., 2006), uncertainty
281 in the reference absorption cross sections used in the retrieval (Stutz and Platt, 1996), and
282 possible distortions of the sensor response function due to temperature or other environmental
283 effects (Galle et al., 2010).

284 The method proposed to derive a representative VCD is based on the assumption that a
285 homogenous layer of gas surrounds the instrument. For each scan that contains a set of 26
286 SCDs taken at steps of 7.2° from horizon to horizon, this assumption results in a trough shape
287 of the distribution of these SCDs. This occurs because the shortest column corresponds to the
288 shortest path through the haze layer, when the scanner looks upwards, and then progressively
289 increases with scan angle, as path length through the haze layer increases (see Figure 4). Thus,
290 the measurements used in this study were selected by visual inspection of each scan, i.e. only
291 scans with the expected trough-shaped distribution of SCDs were used for analysis. In addition,
292 a numerical filter was applied to use only symmetrical scans, where the columns at +60° and -
293 60° differed by less than 20%. A conservative uncertainty related to this method may be 20%,

allowing for imperfect scanning geometry, radiative transfer and natural variability of the columns in the layer. Each VCD thus has a total uncertainty of ~35%.

The uncertainty related to the effective haze width depends on the stability of the wind direction and accuracy in the determination of the dimensions of the lava flow field. The wind direction used here was measured by a meteorological station in close proximity to the scanning system, and these data were in good agreement with measurements from another station operated by IMO 20 km further away. This suggests that wind directions close to ground level were relatively stable over a large area, in spite of the presence of a hot lava flow field and a cold glacier. The accuracy of the effective haze width for different wind directions must also be considered. From a map of the extent of the lava flow field, the maximum widths of the lava flow field in directions perpendicular to wind directions in the range 250° to 290° were measured (Figure 5). This range of wind directions corresponds to the possible directions that would produce a haze above the instrument, which was oriented at 270°. Because our study took place after the eruption had ended, the extent of the lava flow field itself can be considered unchanging. Assuming that the measurements of haze widths from a map can be achieved with an accuracy of 1%, and that wind directions vary (spatially and temporarily) within 20%, the total uncertainty on haze width is of the order of 20%.

Finally, uncertainty related to the haze speed must be determined. It is assumed here that haze speed is equal to wind speed close to ground. We attribute a value of 20% to this uncertainty, following Galle et al., (2002) and Edmonds et al., (2003). Therefore, the total uncertainty of a single flux measurement is estimated to be, quite conservatively, 45%. The total uncertainty is calculated by summing in "quadrature" the uncertainty of all variables, that is, the relative uncertainty of the flux is equal to the square root of the sum of the squares of the relative uncertainties of the variables, i.e. $\sqrt{(0.35^2+0.2^2+0.2^2)} = 0.45$.

Results

Lava flow field SO_2 flux

Post-eruption SO_2 fluxes from the Holuhraun lava flow field were calculated as varying between <1 kg/s and 9 kg/s (Figure 7). In the three months following the eruption, the lava flow field released an average of 3 kg/s of SO_2 (standard deviation: 1.9 kg/s). We found no overall trend in SO_2 emission with time, instead the SO_2 outgassing rate fluctuated without discernible trend during the three month period following the end of the eruption. The flux varied between 2 and 6 kg/s in the first weeks of March, then decreased and varied between 1 and 3 kg/s at the end of March. It became higher (~6 kg/s) and stable in April, then highly fluctuating again (1-9 kg/s) by the end of May 2015. The lack of DOAS scans with the required characteristics (trough-shaped distribution with wind direction blowing towards the instrument) in the first weeks of May and the scarcity of scans in April may reflect the less favourable weather conditions for useful DOAS measurements during the transition between winter and spring seasons.

DOAS data from the Holuhraun eruption were processed until the end of May 2015 (Figure 7), after which SO_2 from the lava flow field was below the detection limit of the instrument (5 ppm*m for single spectra). Thus, the lava flow field formed during a six-month long eruption continued to release measurable SO_2 for three months after the eruption ended.

Contribution of Holuhraun lava flow field SO_2 emissions

339 Assuming that the average post-eruption flux of 3 kg/s was emitted constantly throughout the
340 three months of this study, an estimated total of 24 kt of SO_2 was released during this period.
341 This is equivalent to an additional 0.2% to the total of ~11 Mt of SO_2 that was released during
342 the eruption. This estimated 24 kt of SO_2, released during three months, is greater than the 16
343 kt of SO_2 emitted by Icelandic industry in 2013 (Centre on Emission Inventories and
344 Projections, 2015). The SO_2 emitted by the lava flow field remained near ground level,
345 resulting in high ground-level concentrations of SO_2 near to the eruption site, and posing
346 potential health hazards (including respiratory problems and eye irritation; Longo et al, 2008;
347 Ilyinskaya et al., 2017) to people exposed to it. Access was therefore restricted to the area
348 around the lava flow field until 1 June 2015, after a field visit by IMO on 19 May 2015
349 measured only minor emissions of SO_2 from fractures in the lava and from the main eruption
350 crater (IMO, 2015c).

351 The Holuhraun eruption magma was highly rich in sulphur (Gauthier et al., 2016; Gíslason et
352 al., 2015), resulting in high emissions of SO_2 at the vent. It is likely that the magma had a
353 permeable bubble network during ascent allowing volatiles to be released from the magma to
354 form the gas-rich eruption plume (e.g. Burton et al., 2007; Polacci et al., 2008). Therefore,
355 when the lava was erupted much of its sulphur content had already been released by efficient
356 degassing at the vent, and so only a small proportion of SO_2 remained within the lava to be
357 released during and after emplacement. Due to the large size of this flood basalt eruption, this
358 small proportion of SO_2 released by the lava flow field was still a large and significant mass of
359 SO_2.

360 The petrologic approach of Bali et al. (submitted) was used to calculate the portion of erupted
361 lava responsible for outgassing the post-eruptive SO_2. Degassed tephra glass contained 377
362 ppmw sulphur (Bali et al.), and degassed lava contained 97 ppmw sulphur (Gauthier et al.,

2016). The 24 kt of post-eruptive SO_2 are calculated to have been emitted from 4.23×10^{10} kg of the 3.56×10^{12} kg of lava produced by the Holuhraun eruption.

Lava flow field radiant heat flux

The radiant heat flux due to the Holuhraun lava flow field decreased following the end of the eruption (Figure 8), from 13.3×10^3 MW on 8 February 2015 (in the final month of the eruption) to 6.9×10^3 MW on 10 March (10 days after the eruption ended), followed by a continued cooling. Once the eruption had ended, the source of hot lava was removed, and so all heat released was due to the cooling of the existing lava. The measured post-eruption SO_2 fluxes were emitted as this emplaced lava cooled.

Discussion

Cooling and outgassing of lava flows

Several studies have analysed the cooling and crystallisation of lava bodies (e.g. Keszthelyi and Denlinger, 1996; Wooster et al., 1997; Cashman et al., 1999; Patrick et al., 2004; Kolzenburg et al., 2016). Lava flows cool by thermal radiation and atmospheric convection from the surface, and by conduction to the underlying country-rock (Keszthelyi and Denlinger, 1996; Neri, 1998; Patrick et al., 2004). Lava from the Holuhraun eruption had up to 45% vesicles (Lavallée et al., 2015). This high vesicularity is likely to have enhanced the cooling of the flows as lava porosity is considered to affect the rate of cooling, with more vesicular lava cooling more rapidly (Keszthelyi and Denlinger, 1996).

384 Processes that occur during cooling could contribute to the release of SO_2 from the lava flow.
385 As an emplaced lava flow cools and solidifies post-eruption, it thermally contracts (Spry, 1962;
386 Wittmann et al., 2017). Thermal contraction of lava results in the formation of cooling fractures
387 such as brittle cracks and columnar jointing (Ryan and Sammis, 1978; Long and Wood, 1986;
388 Reiter et al., 1987; Grossenbacher and McDuffie, 1995). Continued cooling causes fractures to
389 propagate from the surface into the interior of the flow (Reiter et al., 1987; Aydin and DeGraff,
390 1988; Kattenhorn and Schaefer, 2008). Not only will fractures and cracks enhance the cooling
391 of the lava flow interior, they will also provide pathways for volatiles to be released from the
392 interior of the flow to the atmosphere (Fuller, 1938; Wilmoth and Walker, 1993).

393 Vesicles within a lava flow consist of both a primary population that were exsolved from the
394 melt during eruption, and a secondary population that were exsolved during cooling and
395 crystallisation (Cashman et al., 1994). The strength of the cooling lava crust will prevent the
396 upward migration of bubbles, causing volatiles to remain trapped within the flow (Polacci and
397 Papale, 1997). Volatiles exsolved from the lava therefore contribute to the formation of a low
398 permeability vesicle network in which the volatiles become trapped, with inefficient outgassing
399 due to the formation of a solid outer crust on the lava flow. The outgassing efficiency will be
400 dependent on the permeability of the lava flow (Burgisser and Degruyter, 2015; Kennedy et al.,
401 2016), with the permeability dependent on vesiculation history (Saar and Manga, 1999; Wright
402 et al., 2009). Fracturing of the lava will then create high permeability pathways allowing
403 efficient outgassing of these trapped volatiles, as seen at the Holuhraun lava flow field (Figure
404 9).

405 Extraction of gas from the lava flow should be most efficient where it is highly fractured, which
406 will be where the thermal contraction is greatest. The formation of high permeability pathways
407 through propagation of cooling fractures would account for the fact that SO_2 was released from

the Holuhraun lava flow field for several months after lava flow emplacement, and that over this time the SO_2 flux did not decrease concurrently with the decrease in thermal emission. SO_2 flux is not a simple decay correlated with lava cooling, as both volatile availability and fracture propagation produce the SO_2 flux. As fractures provide a pathway for gas to escape, outgassing is able to continue as fracture propagation continues to tap volatiles trapped in the cooling flow interior. The episodic nature of fracture propagation (Ryan and Sammis, 1978; DeGraff and Aydin, 1987; Reiter et al., 1987) would explain the fluctuating post-eruption SO_2 flux.

Using a petrological method, Thordarson et al. (1996) calculated that of the SO_2 released by the 1783-1784 Laki eruption, 20% was released by lava flows during their emplacement and cooling. This is two orders of magnitude larger than our calculated value of 0.2% of SO_2 released by the Holuhraun lava flow field in the three months following the eruption. The reason for this large discrepancy is that our measurements only began after the eruption had ended. The Holuhraun eruption lasted for six months, and therefore lava flows had been outgassing for up to six months before our study even began, and so a significant proportion of the outgassing has not been captured. Outgassing from lava flows is likely to have been greatest during emplacement, when mechanical break up of the lava crust facilitated gas release (Polacci and Papale, 1997; Soule and Cashman, 2004), and we did not capture syn-emplacement outgassing during our study.

The hazard caused by the outgassing of the Holuhraun lava flow remained at ground level as SO_2 formed a low-lying haze, and it continued to occur after the eruption ended as the lava flow field continued to outgas.

Conclusions

Remote sensing scanning DOAS instruments were installed at the eruption site of the 2014-2015 Holuhraun eruption to monitor the flux of SO_2. Based on a novel approach to measure emissions from the emplaced lava flow field, we found that this field continued to release SO_2 for three months after the end of the eruption. During this time, SO_2 flux from the lava flow field varied from <1 kg/s to 9kg/s, and a post-eruption average flux of 3 kg/s was calculated. The post-eruption Holuhraun lava flow field was a significant source of environmental pollution, releasing 24 kt of SO_2 in the three months after the eruption. This post-eruption lava flow field SO_2 flux contributed an additional 0.2% to the ~11 Mt total eruption SO_2 emissions in the three months following the eruption. This emission remained near ground level, posing health hazards, which resulted in access to the area being restricted until 1 June 2015, three months after the eruption ended. During solidification, SO_2 can be outgassed, we propose, by fracture propagation as high permeability pathways are developed, allowing gas to be released for several months after the end of the eruption. We show that this release is not a simple decay correlated with lava cooling, as both volatile availability and fracture propagation produce a fluctuating SO_2 flux.

Acknowledgements

The installation of the DOAS instruments at Holuhraun were funded by FUTUREVOLC and a Swedish FORMAS grant (2014-1848). We gratefully thank Baldur Bergsson and staff at the Icelandic Meteorological Office for installing and maintaining the equipment. The NovacProgram software was developed by M. Johansson and Y. Zhang. The authors thank Christoph Kern, Andrew Harris and an anonymous reviewer for their comments and suggestions which have greatly improved this manuscript.

455 **References**

456 Aydin, A., DeGraff, J. M., 1988. Evolution of polygonal fracture patterns in lava flows.
457 Science 239:471-476

458 Barsotti, S., Jóhannsson, T., Hellsing, V. Ú., Pfeffer, M. A., Guðnason, T., Stefánsdóttir,
459 G., 2015. Abundant SO_2 release from the 2014 Holuhraun eruption (Bárðarbunga,
460 Iceland) and its impact on human health. Geophysical Research Abstracts 17 EGU2015-
461 12886

462 Bluth, G. J. S., Shannon, J. M., Watson, I. M., Prata, A. J., Realmuto, V. J., 2007.
463 Development of an ultra-violet digital camera for volcanic SO_2 imaging. J Volcanol
464 Geotherm Res 161:47-56

465 Bobrowski, N., Kern, C., Platt, U., Hörmann, C., Wagner, T., 2010. Novel SO_2 spectral
466 evaluation scheme using the 360-390 nm wavelength range. Atmos Meas Tech 3:879-891

467 Bottinga, Y., Javoy, M., 1991. The degassing of Hawaiian tholeiite. Bull Volcanol 53:73-
468 85

469 Burgisser, A., Degruyter, W., 2015. Magma ascent and degassing at shallow levels. In:
470 Sigurdsson, H., Houghton, B., McNutt, S. R., Rymer, H., Stix, J., (Eds), The
471 Encyclopedia of Volcanoes, second edition

472 Burton, M. R., Mader, H. M., Polacci, M., 2007. The role of gas percolation in quiescent
473 degassing of persistently active basaltic volcanoes. Earth Plan Sci Let 264:46-60

474 Cashman, K. V., Mangan, M. T., Newman, S., 1994. Surface degassing and modification
475 to vesicle size distributions in active basalt flows. J Volcanol Geotherm Res 61:45-68

476 Cashman, K. V., Thornber, C., Kauahikaua, J. P., 1999. Cooling and crystallisation of
477 lava in open channels, and the transition of Pāhoehoe Lava to ‘A’ā. Bull Volcanol
478 61:306-323

479 Centre on Emission Inventories and Projections, European Monitoring and Evaluation
480 Programme, 2015.

481 http://www.ceip.at/ms/ceip_home1/ceip_home/data_viewers/official_tableau/. Accessed
482 3 June 2016

483 Coppola, D., Laiolo, M., Cigolini, C., Delle Donne, D., Ripepe, M., 2016. Enhanced
484 volcanic hot-spot detection using MODIS IR data: results from the MIROVA system. In:
485 Harris, A. J. L., De Groeve, T., Garel, F., Carn, S. A., (Eds.), Detecting, modelling and
486 responding to effusive eruptions. The Geological Society of London, Special
487 Publications, 426:181-205 doi: 10.1144/SP426.5

488 Coppola, D., Ripepe, M., Laiolo, M., Cigolini, C., 2017. Modelling satellite-derived
489 magma discharge to explain caldera collapse. Geology 45(6): 523-526
490 doi:10.1130/G38866.1

491 DeGraff, J. M., Aydin, A., 1987. Surface morphology of columnar joints and its
492 significance to mechanics and direction of joint growth. Geol Soc Am 99:605-617

493 Edmonds, M., Herd, R. A., Galle, B., Oppenheimer, C., 2003. Automated, high time-
494 resolution measurements of SO_2 flux at Soufrière Hills Volcano, Montserrat. Bull Volcanol
495 65:578-586

496 Edner, H., Ragnarson, P., Svanberg, S., Wallinder, E., Ferrara, R., Cioni, R., Raco, B.,
497 Taddeucci., G., 1994. Total fluxes of sulfur dioxide from the Italian volcanoes Etna,
498 Stromboli and Vulcano measured by differential absorption lidar and passive differential
499 optical absorption spectroscopy. J Geophys Res 99:827-838

500 Fuller, R. E., 1938. Deuteric alteration controlled by the jointing of lavas. Am J Sci
501 25:161-171

502 Galle, B., Johansson, M., Rivera, C., Zhang, Y., Kihlman, M., Kern, C., Lehmann, T.,
503 Platt, U., Arellano, S., Hidalgo, S., 2010. Network for Observation of Volcanic and
504 Atmospheric Change (NOVAC) – A global network for volcanic gas monitoring:
505 Network layout and instrument description. J Geophys Res 115
506 doi:10.1029/2009JD011823

507 Galle, B., Oppenheimer, C., Geyer, A., McGonigle, A. J. S., Edmonds, M., Horrocks, L.,
508 2002. A miniaturised ultraviolet spectrometer for remote sensing of SO_2 fluxes: a new
509 tool for volcano surveillance. J Volcanol Geotherm Res 119:241-254

Gauthier, P. J., Sigmarsson, O., Gouhier, M., Haddada, B., Moune, S., 2016. Elevated gas flux and trace metal degassing from the 2014-2015 fissure eruption at the Bárðarbunga volcanic system, Iceland. J Geophys Res. Solid Earth 121:1610-1630 doi:10.1002/2015JB012111

Gíslason, S. R., Stefánsdóttir, G., Pfeffer, M. A., Barsotti, S., Jóhannsson, Th., Galeczka, I., Bali, E., Sigmarsson, O., Stefánsson, A., Keller, N. S., Sigurdsson, Á., Bergsson, B., Galle, B., Jacobo, V. C., Arellano, S., Aiuppa, A., Jónasdóttir, E. B., Eiríksdóttir, E. S., Jakobsson, S., Guðfinnsson, G. H., Halldórson, S. A., Gunnarsson, H., Haddadi, B., Jónsdóttir, I., Thordarson, Th., Riihuus, M., Högnadóttir, Th., Dürig, T., Pedersen, G. B. M., Höskuldsson, Á., Gudmundsson, M. T., 2015. Environmental pressure from the 2014-15 eruption of Bárðarbunga volcano, Iceland. Geochemical Perspective Letters 1:84-93

Grainger, J. F., Ring, J., 1962. Anomalous Fraunhofer Line Profiles. Nature, 193:762

Grossenbacher, K. A., McDuffie, S. M., 1995. Conductive cooling of lava: columnar joint diameter and stria width as functions of cooling rate and thermal gradient. J Volcanol Geotherm Res 69:95-103

Hirabayashi, J., Ohba, T., Nogami, K., 1995. Discharge rate of SO_2 from Unzen volcano, Kyushu, Japan. Geophys Res Let 22:1709-1712

Icelandic Meteorological Office, 2014. Bárðarbunga 2014 – November events, http://en.vedur.is/earthquakes-and-volcanism/articles/nr/3023. Accessed 28 September 2015

Icelandic Meteorological Office, 2015a. Bárðarbunga 2015 – February events, http://en.vedur.is/earthquakes-and-volcanism/articles/nr/3087. Accessed 28 September 2015

Icelandic Meteorological Office, 2015b. Bárðarbunga 2015 – January events, Reiterhttp://en.vedur.is/earthquakes-and-volcanism/articles/nr/3071. Accessed 28 September 2015

Icelandic Meteorological Office, 2015c. Bárðarbunga 2015 – March, April, May http://en.vedur.is/earthquakes-and-volcanism/articles/nr/3122. Accessed 3 July 2017

538 Ilyinskaya, E., Schmidt, A., Mather, T. A., Pope, F. D., Witham, C., Baxter, P.,
539 Jóhannsson, T., Pfeffer, M., Barsotti, S., Singh, A., Sanderson, P., 2017. Understanding
540 the environmental impacts of large fissure eruptions: Aerosol and gas emissions from the
541 2014-2015 Holuhraun eruption (Iceland). Earth and planetary Science Letters 472:309-
542 322

543 Jousset, P., Budi-Santoso, A., Jolly, A. D., Boichi, M., Surono, Dwiyono, S., Sumarti, S.,
544 Hidayati, S., Thierry, P., 2013. Signs of magma ascent in LP and VLP seismic events and
545 link to degassing: An example from the 2010 explosive eruption at Merapi volcano,
546 Indonesia. J Volcanol Geotherm Res 261:171-192

547 Kattenhorn, S. A., Schaefer, C. J., 2008. Thermal-mechanical modelling of cooling
548 history and fracture development in inflationary basalt lava flows. J Volcan Geotherm
549 Res 170:181-197

550 Kennedy, B. M., Wadsworth, F. B., Vasseur, J., Schipper, C. I., Jellinek, A. M., von
551 Aulock, F. W., Hess, K., Russell, J. K., Lavallée, Y., Nichols, A. R. L., Dingwell, D. B.,
552 2016. Surface tension driven processes densify and retain permeability in magma and
553 lava. Earth Plan Sci Let 433:116-124

554 Keszthelyi, L., Denlinger, R., 1996. The initial cooling of pahoehoe flow lobes. Bull
555 Volcanol 58:5-18

556 Kolzenburg, S., Giordano, D., Cimarelli, C., Dingwell, D. B., 2016. In situ thermal
557 characterisation of cooling/crystallising lavas during rheology measurements and
558 implications for lava flow emplacement. Geochimica et Cosmochimica Atca 195:244-258

559 Kyle, P. R., Sybeldon, L. M., McIntosh, W. C., Meeker, K., Symonds, R., 1994. Sulphur
560 dioxide emission rates from Mount Erebus, Antarctica. In: Kyle, P. R., (Ed)
561 Volcanological and environmental studies of Mount Erebus, Antarctica 66. American
562 Geophysical Union 69-82

563 Lavallée, Y., Kendrick, J., Wall, R., von Aulock, F., Kennedy, B., Sigmundsson, F., 2015.
564 Experimental constraints on the rheology and mechanical properties of lava erupted in the
565 Holuhraun area during the 2014 rifting event at Bárðarbunga, Iceland. Geophysical
566 Research Abstracts 17 EGU2015-11544

567 Long, P. E., Wood, B. J., 1986. Structures, textures and cooling histories of Columbia
568 River basalt flows. Geol Soc Am Bull 97:1144-1155

569 Longo, B. M., Rossignol, A., Green, J. B., 2008. Cardiorespiratory health effects
570 associated with sulphurous volcanic air pollution. Public Health 122:809-820

571 Malinconico, L. L., 1979. Fluctuations in SO_2 emission during recent eruptions of Etna.
572 Nature 278:43-45

573 McGonigle, A. J. S., Oppenheimer, C., Galle, B., Mather, T., Pyle, D., 2002. Walking
574 traverse and scanning DOAS measurements of volcanic gas emission rates. Geophys Res
575 Let doi: 10.1029/2002GL015827

576 Moffat, A. J., Millan, M. M., 1971. The applications of optical correlation techniques to
577 the remote sensing of SO_2 plumes using sky light. Atmospheric Environment 5:677-690

578 Mori, T., Burton, M., 2006. The SO_2 camera: a simple, fast and cheap method for ground-
579 based imaging of SO_2 in volcanic plumes. Geophys Res Let 33:L24804
580 doi:10.1029/2006GL027916

581 Mori, T., Mori, T., Kazahaya, K., Ohwada, M., Hirabayashi, J., Yoshikawa, S., 2006. Effect
582 of UV scattering on SO_2 emission rate measurements. Geophys Res Let 33:L17315 doi:
583 10.1029/2006GL026285

584 Neri, A., 1998. A local heat transfer analysis of lava cooling in the atmosphere:
585 application to thermal diffusion-dominated lava flows. J Volcanol Geotherm Res 81:215-
586 243

587 Palma, J. L., Blake, S. Calder, E. S., 2011. Constraints on the rates of degassing and
588 convection in basaltic open-vent volcanoes. Geochem Geophys Geosyst 12 Q11006
589 doi:10.1029/2011GC003715

590 Palma, J. L., Calder, E. S., Basualto, D., Blake, S., Rothery, D. A., 2008. Correlations
591 between SO_2 flux, seismicity and outgassing activity at the open vent of Villarrica
592 volcano, Chile. J Geophys Res 113 B10201 doi:10.1029/2008JB005577

593 Patrick, M. R., Dehn, J., Dean, K., 2004. Numerical modelling of lava flow cooling
594 applied to the 1997 Okmok eruption: Approach and analysis. J Geophys Res 109 B03202
595 doi:10.1029/2003JB002537

596 Pedersen, G. B. M., Höskuldsson, Á., Dürig, T., Thordarson, T., Jónsdóttir, I., Riihuus,
597 M. S., Óskarsson, B. V., Dumont, S., Magnusson, E., Gudmundsson, M. T.,
598 Sigmundsson, F., Drouin, V. J. P. B., Gallagher, C., Askew, R., Gudnason, J., Moreland,
599 W. M., Nikkola, P., Reynolds, H. I., Schmith, J., the IES eruption team, 2017. Lava field
600 evolution and emplacement dynamics of the 2014-2015 basaltic fissure eruption at
601 Holuhraun, Iceland. J Volcan Geotherm Res 340:155-169

602 Platt, U., Lübcke, P., Kuhn, J., Bobrowski, N., Prata, F., Burton, M., Kern, C, 2015.
603 Quantitative imaging of volcanic plumes – Results, needs, and future trends. J Vol
604 Geotherm Res 300:7-21

605 Platt, U., Perner, D., Pätz, H. W., 1979. Simultaneous measurement of atmospheric
606 CH_2O, O_3, and NO_2 by differential optical absorption. J Geophys Res 84:6329-6335

607 Platt, U., Stutz, J., 2008. Differential Absorption Spectroscopy. In: Platt, U., Stutz, J.,
608 Differential Optical Absorption Spectroscopy, Physics of Earth and Space Environments,
609 135-174 doi: 10.1007/978-3-540-75776-4_6

610 Polacci, M., Baker, D. R., Bai, L., Mancini, L., 2008. Large vesicles record pathways of
611 degassing at basaltic volcanoes. Bull Volcanol 70:1023-1029 DOI 10.1007/s00445-007-
612 0184-8

613 Polacci, M., Papale, P., 1997. The evolution of lava flows from ephemeral vents at Mount
614 Etna: Insights from vesicle distribution and morphological studies. J Volcanol Geotherm
615 Res 76:1-17

616 Reiter, M., Barroll, M. W., Minier, J., Clarkson, G., 1987. Thermo-mechanical model for
617 incremental fracturing in cooling lava flows. Tectonophysics 142:241-260

618 Ryan, M. P., Sammis, C. G., 1978. Cyclic fracture mechanisms in cooling basalt. Geol
619 Soc Am 89:1295-1308

620 Saar, M. O., Manga, M., 1999. Permeability-porosity relationship in vesicular basalts.
621 Geophys Res Let 26:111-114

622 Sawyer, G. M., Carn, S. A., Tsanev, V. I., Oppenheimer, C., Burton, M., 2008.
623 Investigation into magma degassing at Nyiragongo volcano, Democratic Republic of the
624 Congo. Geochem Geophys Geosyst 9:Q02017 doi:10.1029/2007GC001829

625 Schmidt, A., Leadbetter, S., Theys, N., Carboni, E., Witham, C. S., Stevenson, J. A.,
626 Birch, C. E., Thordarson, T., Turnock, S., Barsotti, S., Delaney, L., Feng, W., Grainger,
627 R. G., Hort, M. C., Höskuldsson, Á., Ialongo, I., Ilinskaya, E., Jóhannsson, T., Kenny, P.,
628 Mather, T. A., Richards, N. A. D., Shepherd, J., 2015. Satellite detection, long-range
629 transport and air quality impacts of volcanic sulphur dioxide from the 2014-2015 flood
630 lava eruption at Bárðarbunga (Iceland). J Geophys Res-Atmos 120
631 doi:10.1002/2015JD023638

632 Soule, S. A., Cashman, K. V., 2004. The mechanical properties of solidified polyethylene
633 glycol 600, an analogue for lava crust. J Volcanol Geotherm Res 129:139-153

634 Sparks, R. S. J., 2003. Dynamics of magma degassing. In: Oppenheimer, D., Pyle, D.,
635 Barclay, J., (Eds), Volcanic Degassing, Geol Soc Spec Publ 213:5-22

636 Sparks, R. S. J., Pinkerton, H., 1978. Effect of degassing on rheology of basaltic lava.
637 Nature 276:385-386

638 Spry, A., 1962. The origin of columnar jointing, particularly in basalt flows. J Geol Soc
639 Australia 8:191-216 DOI: 10.1080/14400956208527873

640 Stoiber, R. E., Malinconico, L. L., Williams, S. N., 1983. Use of the Correlation
641 Spectrometer at volcanoes. In: Tazieff, H., Sabroux, J (Eds) Forecasting Volcanic Events.
642 Elsevier, 425-444

643 Stutz, J., Platt, U., 1996. Numerical analysis and estimation of the statistical error of
644 differential optical absorption spectroscopy measurements with least-squares methods.
645 Applied Optics 35:6041-6053

646 Swanson, D. A., Fabbi, B. P., 1973. Loss of volatiles during fountaining and flowage of
647 basaltic lava at Kilauea volcano, Hawaii. J Res US Geol Surv 1:649-658

Thordarson, T., Larsen, G., 2007. Volcanism in Iceland in historical time: Volcano types, eruption styles and eruptive history. J Geodyn 43:118-152

Thordarson, T., Self, S., 2003. Atmospheric and environmental effects of the 1783-1784 Laki eruption: A review and reassessment. J Geophys Res 108:D1 doi:10.1029/2001JD002042

Thordarson, T., Self, S., Miller, D. J., Larsen, G., Vilmundardóttir, E. G., 2003. Sulphur release from flood lava eruptions in the Veidivötn, Grímsvötn and Katla volcanic systems, Iceland. In: Oppenheimer, C., Pyle, D. M., Barclay, J., (Eds.) Volcanic Degassing. The Geological Society of London, Special Publications, 213:103-121

Thordarson, T., Self, S., Óskarsson, N., 1996. Sulphur, chlorine and fluorine degassing and atmospheric loading by the 1783-1784 AD Laki (Skaftár Fires) eruption in Iceland. Bull Volcanol 58:205-225

Umhverfisstofnun, 2016. http://www.ust.is/default.aspx?pageid=14da32aa-8362-4378-a165-d3a2a6d6f1c6&station=reydarfjordur1hjallaleira. Accessed 17 June 2016

Walker, G. P. L., 1989. Spongy pahoehoe in Hawaii: a study of vesicle-distribution patterns in basalt and their significance. Bull Volcanol 51:199-209

Weibring, P., Edner, H., Svanberg, S., Cecchi, G., Pantani, L., Ferrara, R., Caltabiano, T., 1998. Monitoring of volcanic sulphur dioxide emissions using differential absorption lidar (DIAL), differential optical absorption spectroscopy (DOAS), and correlation spectroscopy (COSPEC). Applied Physics 67:419-426

Wilmoth, R. A., Walker, G. P. L., 1993. P-type and S-type pahoehoe: a study of vesicle distribution patterns in Hawaiian lava flows. J Volcanol Geotherm Res 55:129-142

Wittmann, W., Sigmundsson, F., Dumont, S., Lavallée, Y., 2017. Post-emplacement cooling and contraction of lava flows: InSAR observations and a thermal model for lava fields at Hekla volcano, Iceland. J Geophys Res Solid Earth 122:946-965 doi:10.1002/2016JB013444

674 Wooster, M. J., Wright, R., Blake, S., Rothery, D. A., 1997. Cooling mechanisms and an
675 approximate thermal budget for the 1991-1993 Mount Etna lava flow. Geophys Res Let
676 24:3277-3280

677 Wooster, M. J., Zhukov, B., Oertel, D., 2003. Fire radiative energy for quantitative study
678 of boimas burning: derivation from the BIRD experimental satellite and comparison to
679 MODIS fire products. Remote Sens Environ 86:83-107

680 Wright, H. M. N., Cashman, K. V., Gottesfeld, E. H., Roberts, J. J., 2009. Pore structure
681 of volcanic clasts: Measurements of permeability and electrical conductivity. Earth Planet
682 Sc Lett 280:93-104

683

684

685

686

687

688

689

690

691

692

693

694

Figures and captions

Fig. 1 **a)** Map of Iceland showing the location of the eruption (triangle). **b)** The location of the 2014-2015 Holuhraun eruption site. The fissure is represented by the dashed line and the area of the lava flow field is highlighted. The location of ScanDOAS instrument MAYP111126 is indicated by the symbol **x**. The viewing direction (arrow) and scanning sector (arc segment) of the instrument are shown. Base maps from the Icelandic Meteorological Office (IMO), 2015b

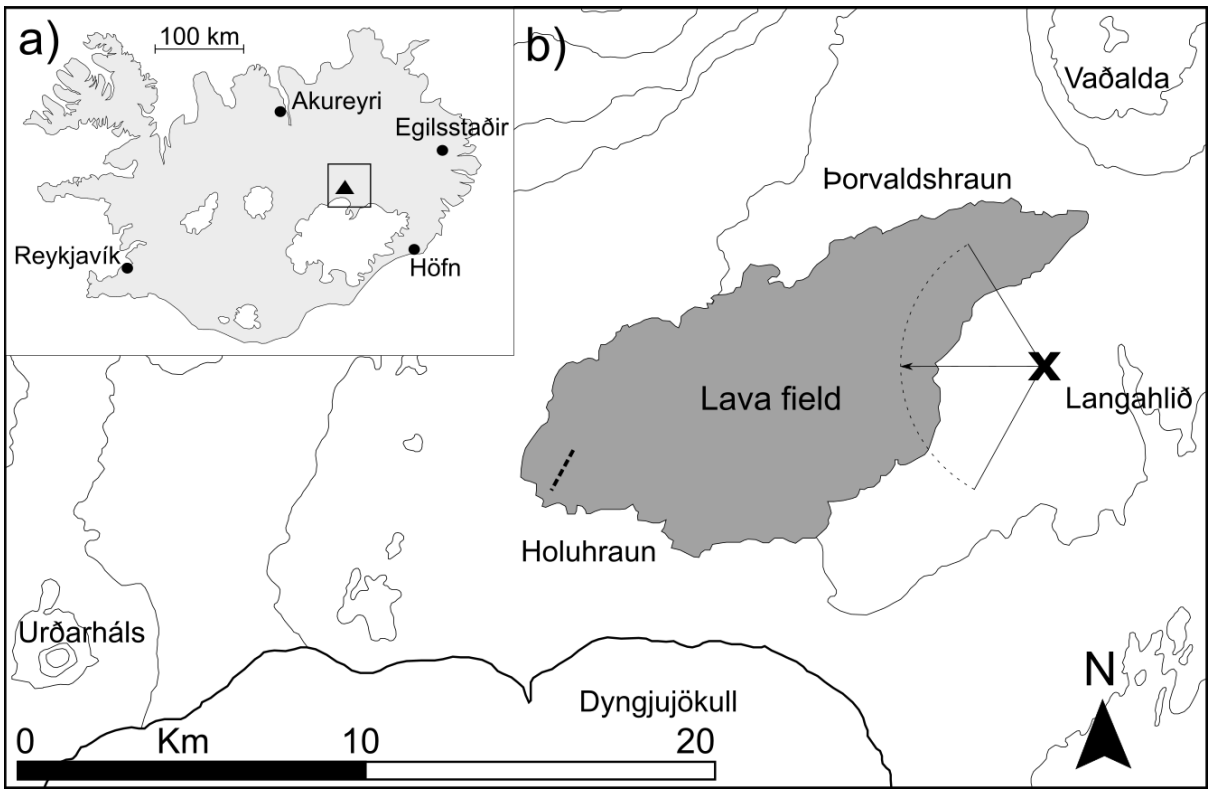

Fig. 2 Two-stage degassing during basaltic fissure eruptions: SO_2 is released at vents contributing to an eruption plume and from lava flows forming a low-level haze. Adapted from Thordarson and Self, 2003. Inset images show **a)** the Holuhraun eruption plume and **b)** gas released by the lava flow field. Photos by B. Bergsson (IMO)

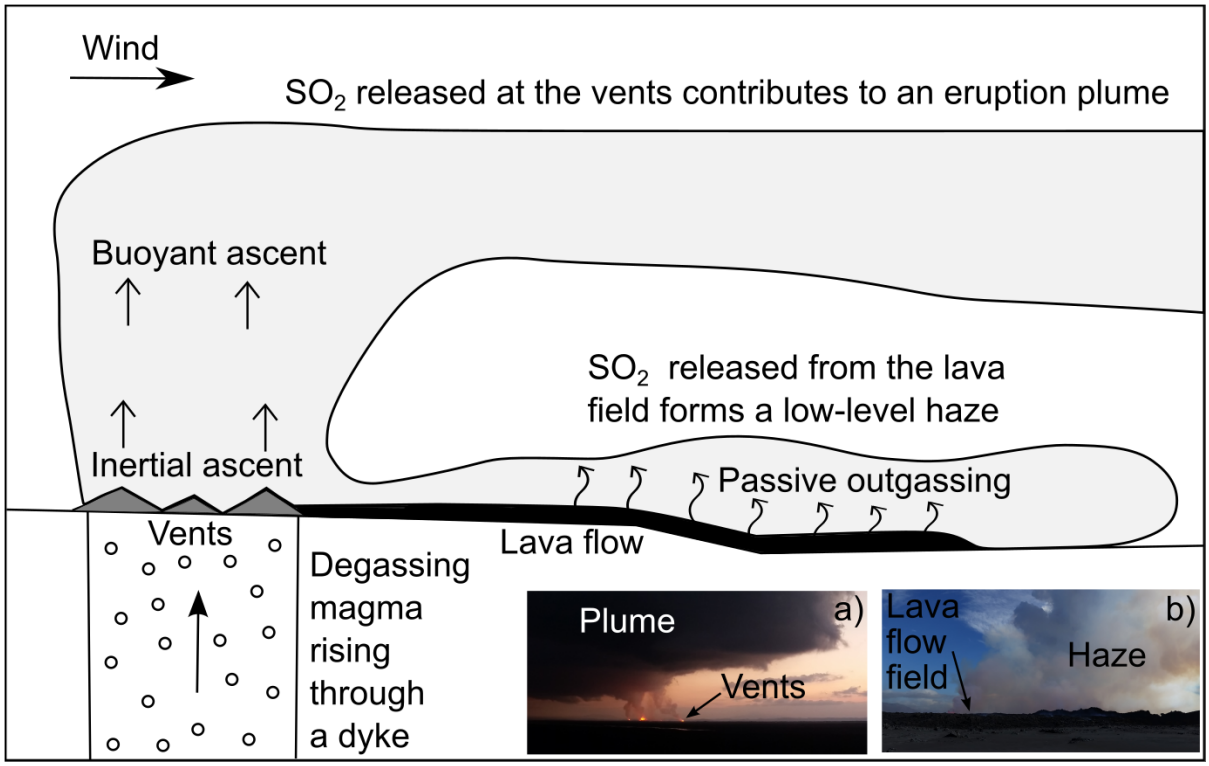

718 **Fig. 3** A photo taken during the surveillance flight on 4th November 2014 showing the low-
719 level gas haze and the higher-level eruption plume. Gases (including H_2O, both magmatic
720 and meteoric, SO_2 and CO_2) can be seen rising from fractures in the lava flow field. Photo by
721 M. Hensch, IMO

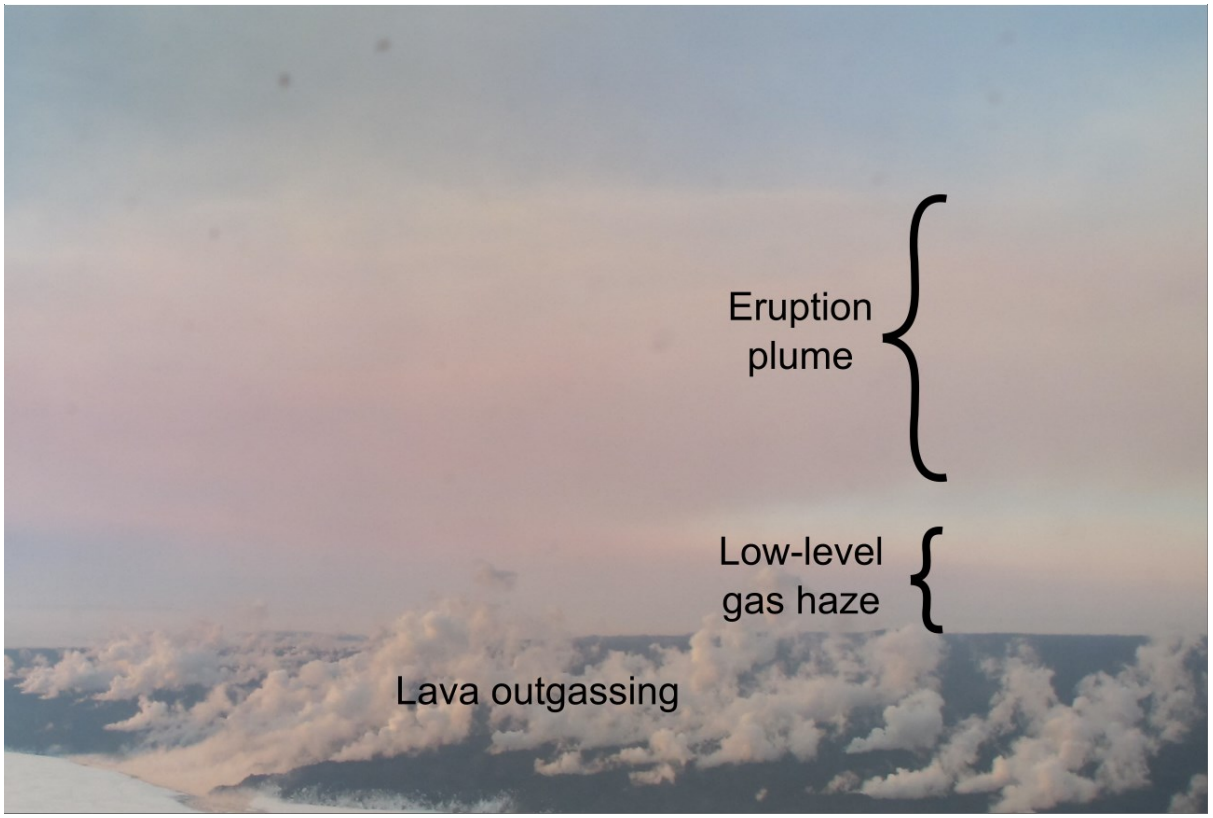

722

723

724

725

726

727

728

729 **Fig. 4** A schematic illustration of the characteristic shapes recorded by scanning DOAS
730 when scanning vertically through **a)** an elevated eruption plume produced by SO_2 released at
731 a vent, and **b)** a low-level haze produced by SO_2 released from a lava flow. **c)** DOAS scan
732 from 11:57 on 7th March 2015 showing the characteristic trough shape of a scan made
733 through the low-level SO_2 haze released by the Holuhraun lava flow field. Black columns are
734 the SO_2 column densities at incremental angles

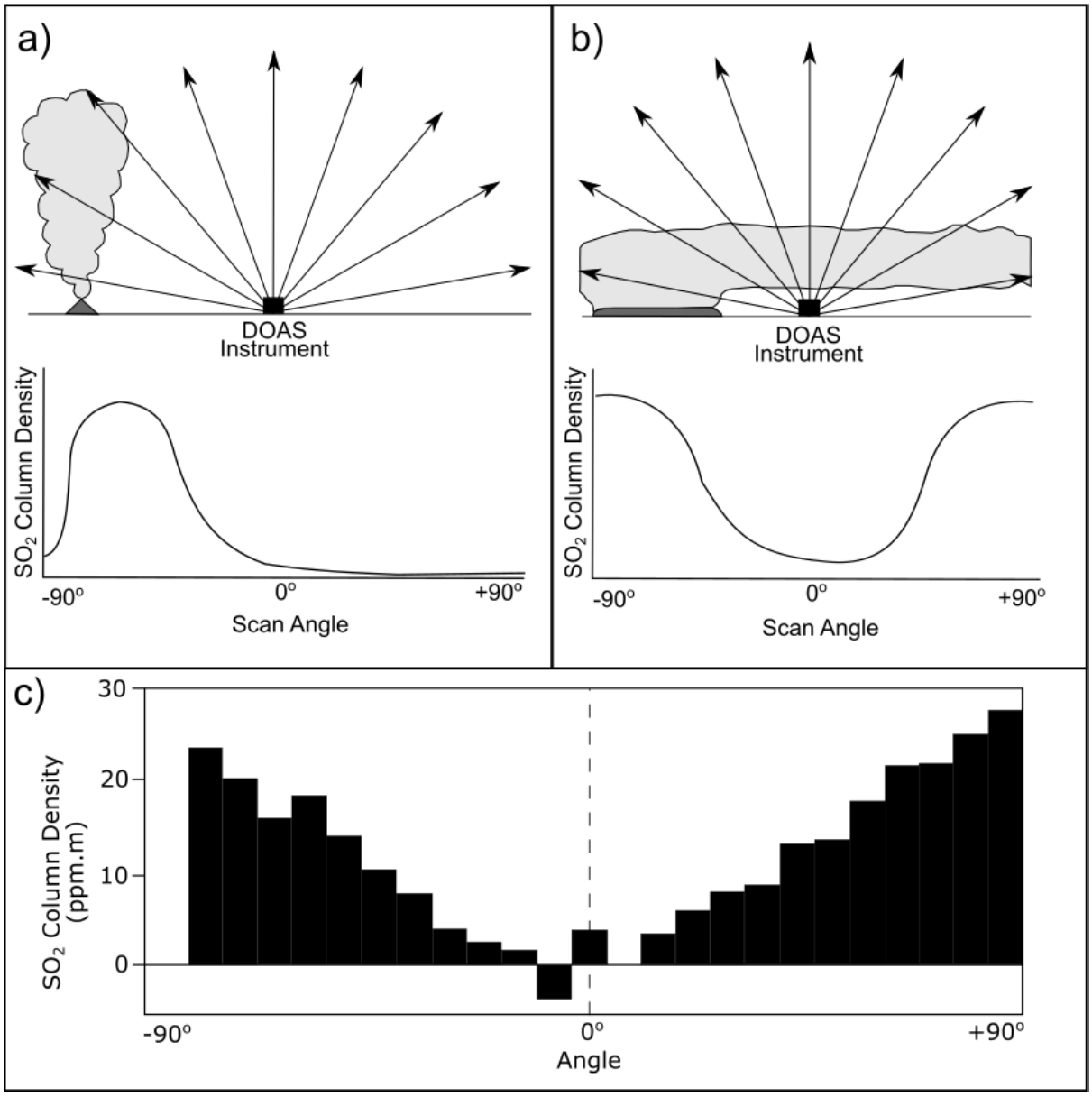

735

736

737 **Fig. 5** The effective plume width (L) is the maximum width of the lava flow field in the
738 direction perpendicular to the wind direction. The diagram shows the effective plume widths
739 (dashed lines) for wind directions (arrows) of 250°, 270° (directly towards the viewing
740 direction of the ScanDOAS instrument) and 290°. The location of ScanDOAS instrument
741 MAYP111126 is indicated by the symbol **x**

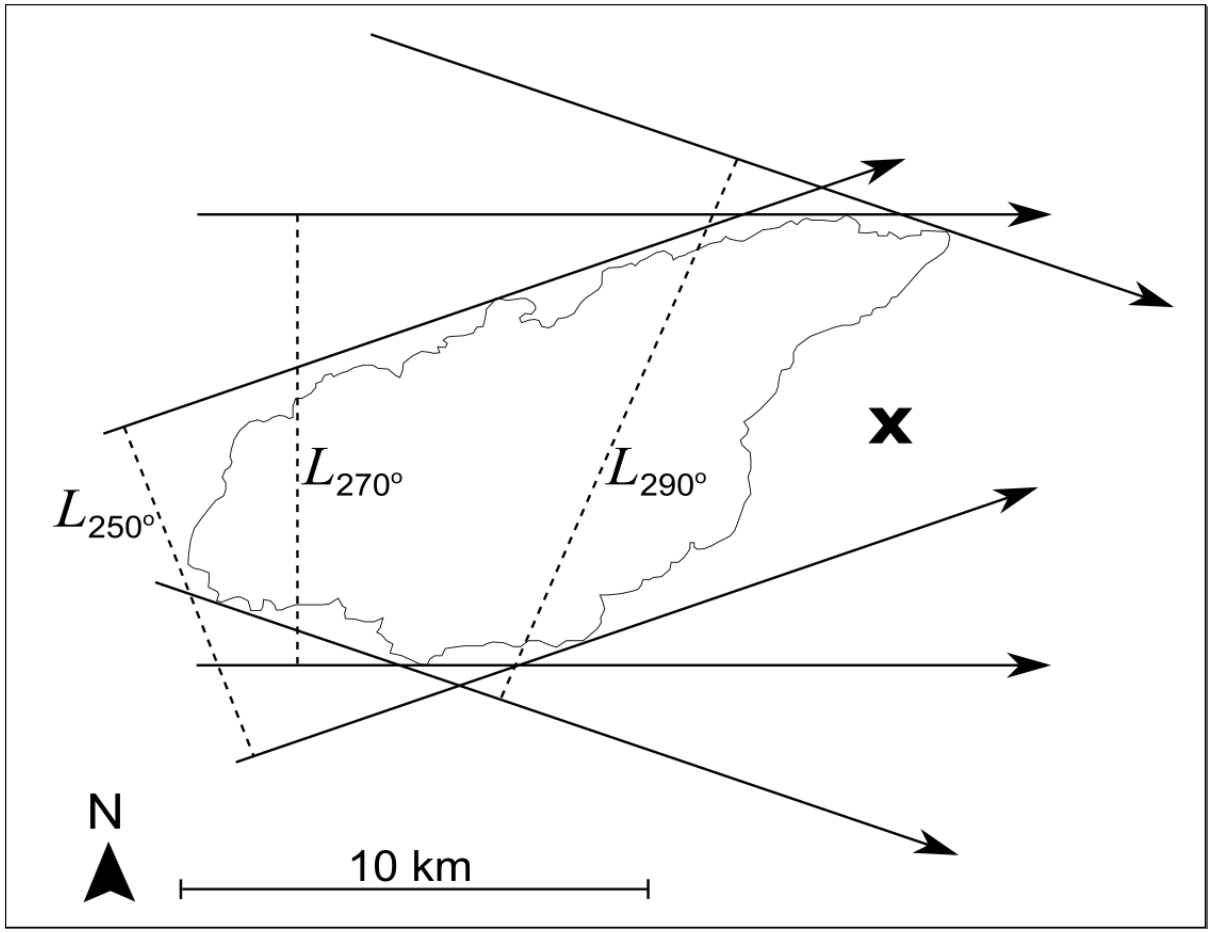

742

743

744

745

746

747 **Fig. 6** A MODIS-MIROVA thermal map (1 km resolution) elaborated for radiant flux
748 calculation during the cooling phase. The map represents the brightness temperature (in K)
749 recorded by the MIR channel of MODIS (centred at ~3.9 μm). Note the temperature anomaly
750 due to the presence of the Holuhraun lava flow field to the south of Askja caldera

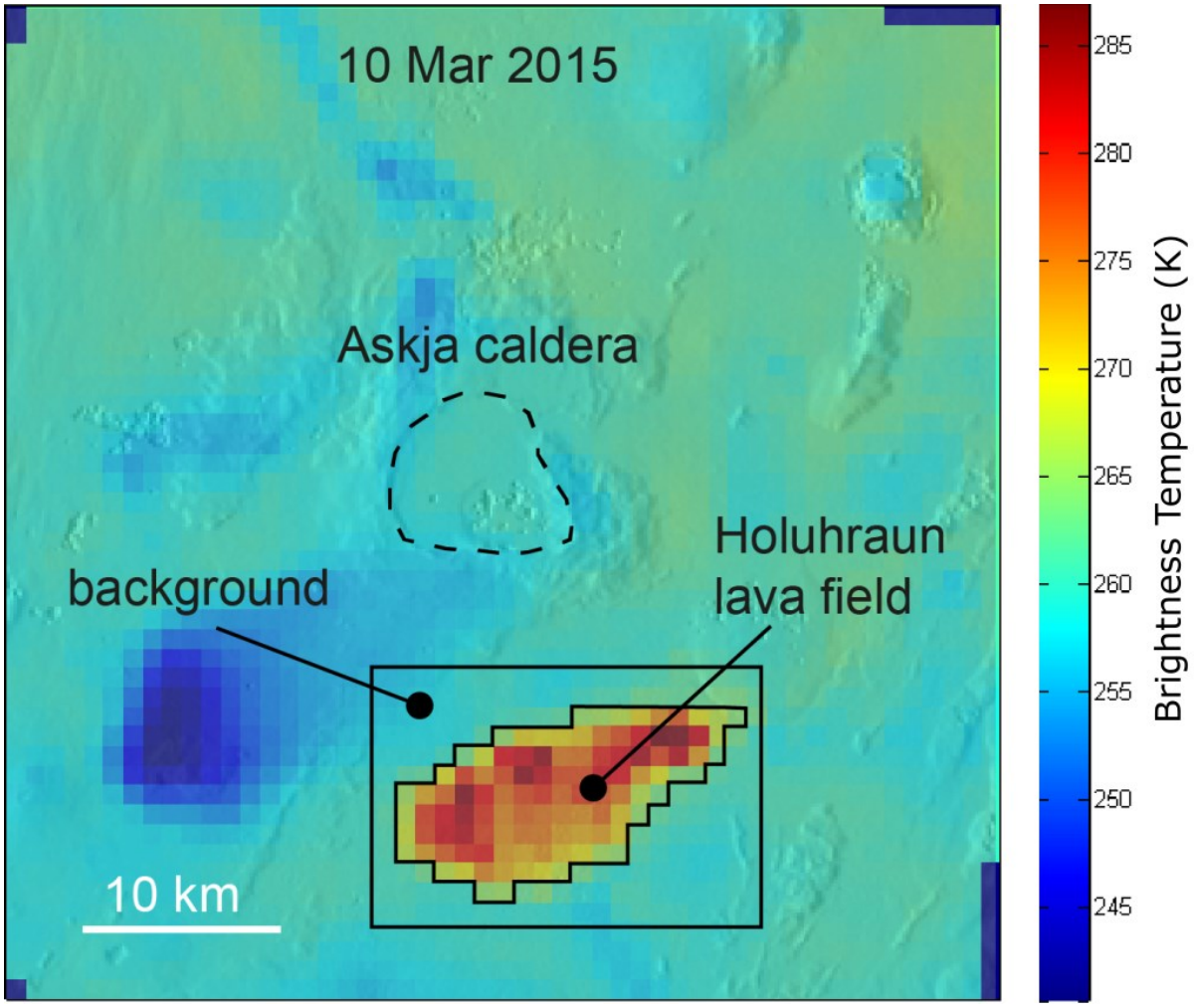

751

752

753

754

Fig. 7 Post-eruption SO_2 flux from the 2014-2015 Holuhraun lava flow field as recorded by ScanDOAS instrument MAYP111126. Labelled dates are at 10 day intervals, error bars are 45%

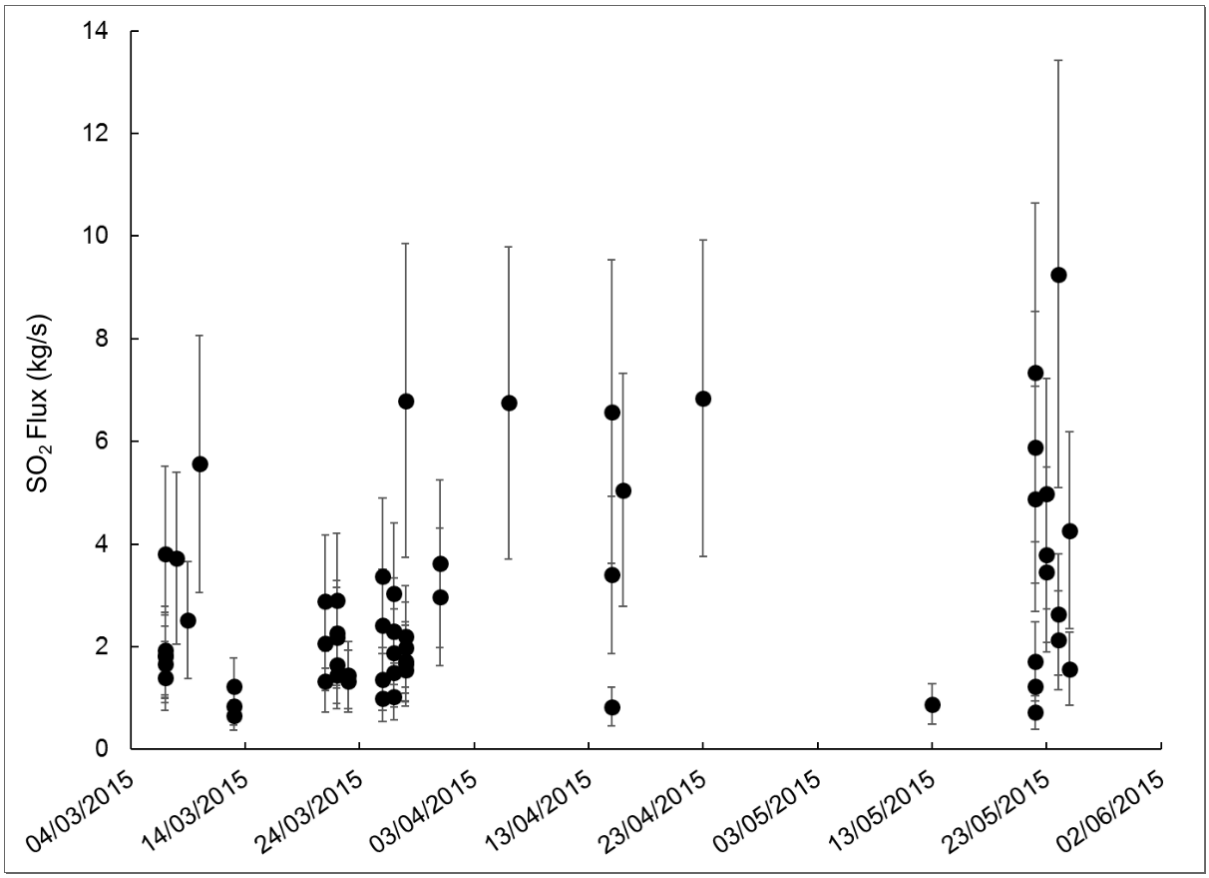

764 **Fig. 8** Radiant heat flux calculated during the post-eruptive cooling phase of the Holuhraun
765 lava flow field according to equation 4. The vertical dashed line indicates the end of the
766 eruption on 27th February 2015. Labelled dates are at 50 day intervals

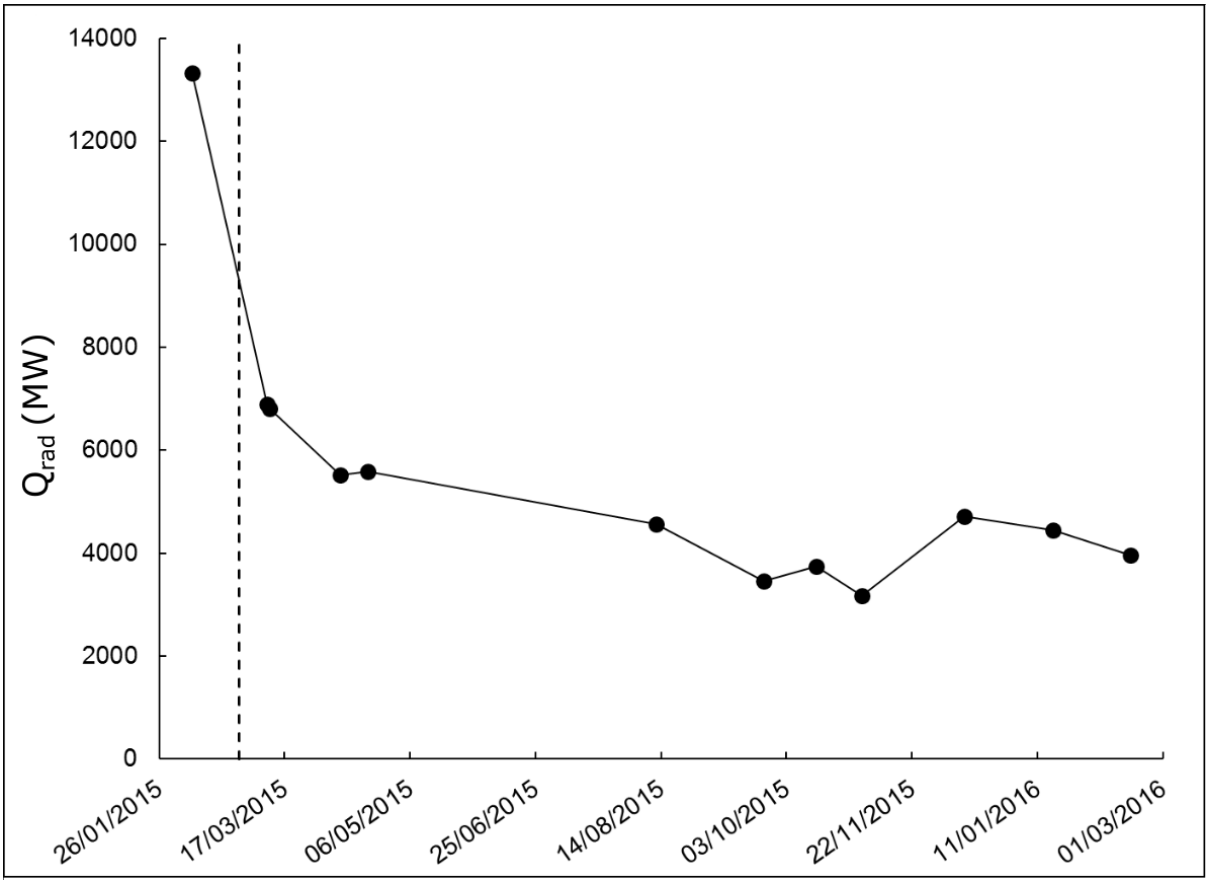

767

768

769

770

771

772

773 **Fig. 9** A photo taken during a surveillance flight on 4th November 2014 showing gases being
774 released from cooling fractures in the lava flow field (highlighted by arrows). Gases include
775 H_2O (both magmatic and meteoric), SO_2 and CO_2. Photo by M. Hensch, IMO

776